Thermal Characterizations of a Lithium Titanate OxideBased LithiumIon Battery Focused on Random and Periodic Charge Discharge Pulses

Madani, Seyed Saeed; Schaltz, Erik; Kær, Søren Knudsen

Published in:
Applied System Innovation

DOI (link to publication from Publisher):
10.3390/asi4020024

Publication date:
2021

Document Version
Publisher's PDF, also known as Version of record

applied system innovation

MDPI

Article

Thermal Characterizations of a Lithium Titanate Oxide-Based Lithium-Ion Battery Focused on Random and Periodic Charge-Discharge Pulses

Seyed Saeed Madani *, Erik Schaltz and Søren Knudsen Kær

Department of Energy Technology, Aalborg University, DK-9220 Aalborg, Denmark; esc@et.aau.dk (E.S.); Skk@et.aau.dk (S.K.K.)

* Correspondence: ssm@et.aau.dk

Abstract: Thermal characterization of lithium-ion batteries is essential to improve an efficient thermal management system for lithium-ion batteries. Besides, it is needed for safe and optimum application. The investigated lithium-ion battery in the present research is a commercially available lithium titanate oxide-based lithium-ion battery, which can be used in different applications. Different experimental facilities were used to measure lithium-ion battery heat generation at different operating conditions and charge and discharge rates in this investigation. Isothermal battery calorimeter is the exclusive calorimeter globally, suitable for lithium-ion batteries' accurate thermal measurements. Pulse charge and discharge in different increments of state of charge were applied to the lithium titanate oxide-based lithium-ion battery to designate the heat generation of the lithium-ion battery cell. Three different cases were studied. The precise effects of different state-of-charge levels and current-rates on lithium-ion battery total generated heat was investigated. The maximum heat generation during 13 A, 40 A, 50 A, 60 A and 100 A pulse discharges were 0.231 Wh, 0.77 Wh, 0.507 Wh, 0.590 Wh and 1.13 Wh correspondingly. It could be inferred that in the case of periodic charge and discharge pulses applied to the lithium titanate oxide-based lithium-ion battery, important parameters including state of charge, current rates, initial cycling, and temperature have a significant influence on total generated heat.

Keywords: lithium titanate oxide-based lithium-ion battery; thermal characterizations

Citation: Madani, S.S.; Schaltz, E.; Kær, S.K. Thermal Characterizations of a Lithium Titanate Oxide-Based Lithium-Ion Battery Focused on Random and Periodic Charge-Discharge Pulses. *Appl. Syst. Innov.* **2021**, *4*, 24. https://doi.org/10.3390/asi4020024

Academic Editor: Evangelos Bellos

Received: 24 February 2021
Accepted: 23 March 2021
Published: 26 March 2021

1. Introduction

With quickly developing energy requirements, there is a significant growth in the need for further renewable and efficient energy resources. Many applications depend on fossil fuels for the furthermost of their energy requirements [1,2]. The combustion of fossil fuels causes the release of greenhouse gases in the direction of the atmosphere. Renewable supplies such as wind energy and solar energy are green supplies of energy. Nevertheless, these are periodic sources. Especially for a continuing application, the storage of energy is essential [3,4]. Lithium-ion batteries are a considerably essential element of electric vehicles. Their application has enhanced noticeably in the last few years [5]. Lithium-ion batteries are the most attractive energy storage technology for different utilizations. The aforementioned is attributable to their rapid discharge and charge capability, big scalability and efficiency, great energy and power density [6,7].

Lithium-ion battery discharging and charging characteristics are intensely dependent on its working temperature. The lithium-ion battery's performance is influenced by the lithium-ion battery's charge transfer resistance [8]. It was demonstrated that lithium-ion batteries' electrical performance depends significantly on the working temperature, with a decline of almost ninety-five percent in energy density for the lithium-ion batteries at −40 °C while in comparison with the identical discharge rate at 20 °C [9]. A significant dependence of solid electrolyte interface resistance and electrolyte resistance on lithium-ion

battery temperature was showed. Both of which influence ion diffusion resistance and charge transfer [10]. An immense correspondence between lithium-ion battery performance and the temperature was found. A growth in lithium-ion battery performance attributable to more immense raised ionic conductivity and salts' diffusion rate at more significant lithium-ion battery temperatures was found [11].

The cycling and thermal behaviors of a lithium titanate-based lithium-ion pouch cell were investigated. The titanate-based lithium-ion cell demonstrated a considerably temperature-dependent capacity. The cell showed excellent capacity retention and excellent internal resistance stability, indicating exceptional lithium titanate's stability as anode material [12]. Essential heat transfer and finite element investigation tools were used to forecast the temperature distributions in cells and modules. Liquid crystal thermography and infrared photography were used to acquire thermal pictures of the lithium-ion battery modules' surface [13].

The thermal characterization and cooling of lithium-ion batteries were accomplished. Recognition of the thermal field was done through thermographic experiments throughout electric discharging and charging. The goal was to assess the cooling requirement throughout the conventional working of an electric vehicle [14]. A finite element investigation approach was used to assess the packs' thermal behavior and modules regarding their geometry. Dissimilar thermal modeling procedures were used to determine thermal performance and the influence of temperature on vehicle performance. The thermal model simulation was done in the ADVISOR tool. The battery thermal model was combined with its battery performance models. The model could forecast the temperature alterations in a vehicle's battery corresponding to the drive cycle [15].

A novel transient approach for quantifying the thermal parameters of a lithium-ion battery was developed. Optimization and finite element modeling were used. The lithium-ion battery's heat generation rate was determined under various states of charge and temperature [16]. For the automotive implementations, lithium-ion batteries are restricted by gravimetric and volumetric energy density, accompanied by cycle life. With superior construction of the electrode magnitude, mechanical, and shape properties, there are many advancement opportunities. It is usually appropriately comprehended that enhancing the working temperature of a lithium-ion battery tends to raise the degradation rate [17–21].

The lithium-ion battery's spatial temperature difference could reason the state of charge drift and differences in current densities attributable to the temperature dependency of both the open circuit potential and proportion of discharge to charge pulse impedance [22]. Different investigations have been accomplished to determine the charge and discharge capabilities of different lithium-ion battery chemistries to enhance precision in the state of charge approximation and characterize lithium-ion battery performance at different temperatures [23,24]. Different methods, including calorimetry, were used for thermal analysis of small lithium-ion batteries [25–29]. Throughout the working of the lithium-ion batteries, heat is generated within the lithium-ion batteries. Therefore, comprehension of heat generation is essential in diminishing the significant temperature effects in lithium-ion batteries.

The irreversible part of heat generation is a sophisticated parameter to be calculated and is characterized in various procedures in dissimilar heat analyzing models and was employed for lithium-ion battery heat generation modeling. Dissimilar procedures were used for the determination of entropic. In [30], a specific load profile and thermal cycles were applied to the lithium-ion battery cell, and potentiometry was employed to approximate this heat coefficient. In [31], the effect of discharge current-rates and state-of-charge on the heat loss and efficiency of a lithium-ion battery was studied. The discharge current pulse step period was set to a ten percent state of charge. The incorporation of the heat flux throughout the stepped procedure gives in to the lithium-ion battery heat generation.

In [32], reversible heat and irreversible heat sources were considered two principal sources of lithium-ion battery heat generation. The entropic heat coefficient was determined to estimate the heat generation within the lithium-ion battery. The reversible part of the

heat generation rate was calculated from the entropy difference. The irreversible part of heat generation was calculated by use of current rate and internal resistance. In [33,34], a lithium titanate oxide-based lithium-ion battery's thermal behavior and thermal behavior were studied under fast discharging and charging conditions by using an isothermal battery calorimeter. The previous investigations focused on understanding the lithium-ion battery's heat generation behavior during full charge and discharge cycles.

Several researchers analyzed the thermal behavior and heat generation of lithium-ion batteries. A comprehensive list of all these attempts is available in Table 1. As demonstrated in the literature review, the prior studies on the heat generation measurement of lithium-ion batteries demonstrate extensive outcomes. Nevertheless, not many research papers have studied the heat generation rates of lithium-ion batteries suitable for different applications. In addition, less attention was paid to thermal characterizations of lithium titanate oxide-based lithium-ion batteries.

Table 1. Literature overview on heat generation measurements of lithium-ion batteries.

Ref.	Investigation	Heat Generation Measurement Method	Battery Type	Discharge Rate	Highest Heat Generation
[35]	Electro-thermal model	Adiabatic calorimeter	LFP/graphite	1 C, 3 C, 5 C	1.17 W (1 C) 7.19 W (3 C) 17.95 W (5 C)
[36]	Thermal modeling of big cells	Adiabatic calorimeter	LCO/graphite	1 C, 3 C, 5 C	3.1 W (1 C) 14 W (3 C) 28 W (5 C)
[37]	Potentiometric and calorimetric measurement of entropy changes	Isoperibolic calorimeter	NMC/carbon	0.5 C, 1 C, 1.5 C	0.332 kJ (0.5 C) 0.798 kJ (1 C) 1.485 kJ (1.5 C)
[38]	Heat generation in high power battery	Adiabatic calorimeter	NMC/graphite	1 C, 2 C	11 W (1 C) 33 W (2 C)
[39]	Theoretical and experimental analysis of heat generations	Isothermal calorimeter	LMO/carbon	4.1 C, 5 C, 5.7 C, 6.3 C,7 C	15 W (4.1 C) 22 W (5 C) 30 W (5.7 C) 35 W (6.3 C) 40 W (7 C)
[40]	Thermal characteristics	Temperature sensors and an aluminum heat sink	$Li_xMn_2O_4$ Spinel	0.1 C, 0.2 C, 0.33 C, 1 C	0.82 W/L (0.1 C–0.2 C) 0.97 W/L (0.2 C–0.5 C) 3.21 W/L (0.5 C–1 C)
[41]	Characterization using electrochemical–calorimetric measurements	Accelerated rate calorimeter	Li-ion batteries	0.1 C, 0.33 C	0.26 W/L
[42]	Electrochemical-calorimetric studies	Accelerated rate calorimeter	cylindrical Li-ion battery	0.33 C, 0.5 C, 1 C	1.63 W/L

2. Experimental

An isothermal battery calorimeter measures heat energy, which is removed under isothermal conditions. The generated heat during the reaction is measured and transferred with the intention of keeping the temperature of the sample constant. Nevertheless, some error could be produced from the system's elevated capacity attributable to the surrounding lithium-ion battery chamber. Maccor automated test system was used as the lithium-ion battery cycler. Calibration of the isothermal battery calorimeter comprises several electrical currents to an accurate resistance, which should be positioned inside the isothermal battery calorimeter. The investigated lithium-ion battery cell capacity is 13 Ah and possesses a lithium titanate oxide-based anode from altairnano. A specific fixture was designed for the lithium-ion battery, which refrains from expansion in the lithium-ion battery cell

volume caused by working with significant current rates and significant temperatures. Experimental facilities which were used in this investigation are illustrated in Figure 1.

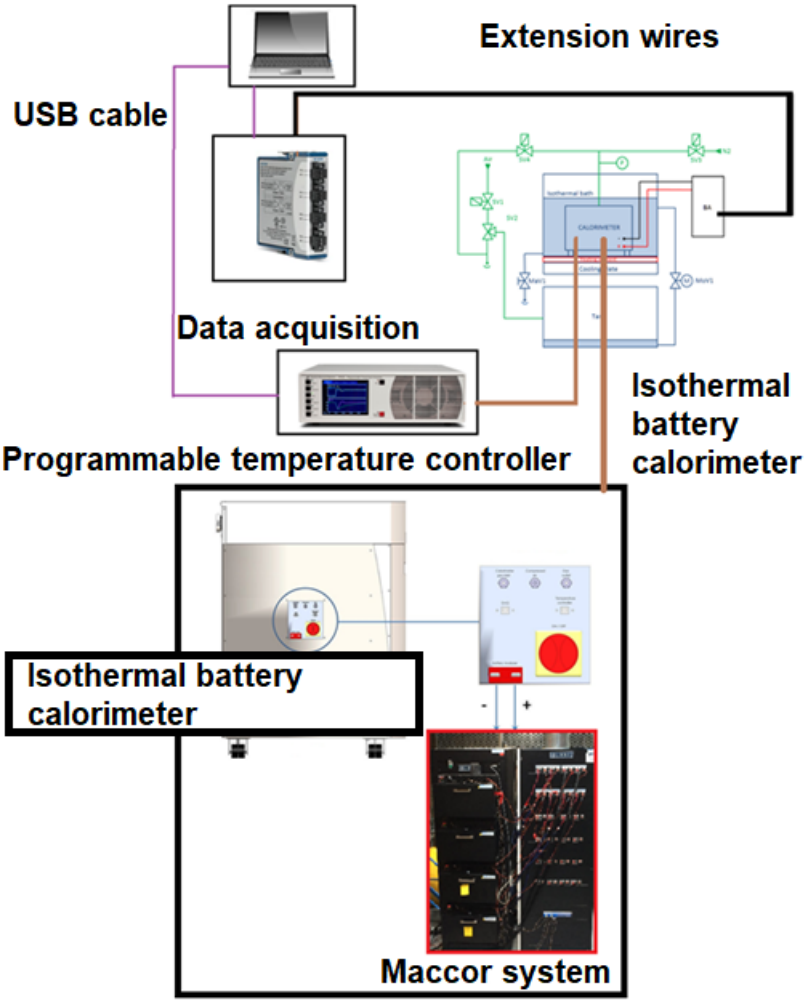

Figure 1. Experimental facilities.

3. Result

The heat produced within a lithium-ion battery arisen from an amalgamation of the reversible and irreversible heat fluxes. These are owing to entropy change and ohmic losses correspondingly. The origin of lithium-ion batteries heat generation and solution approach for heat transfer of lithium-ion batteries is described in Figure 2. In the lithium titanate oxide-based lithium-ion cell surface, thermal energy is dissipated from the lithium-ion battery to the surroundings by natural convection and radiation attributable to the temperature variation between the environment and lithium-ion battery surface. Three different cases were considered for thermal analysis of the lithium titanate oxide-based lithium-ion battery. Different tests were exerted on a 13 Ah lithium titanate oxide battery cell using an isothermal battery calorimeter and Maccor system to comprehend lithium-ion batteries' thermal behavior subject to dissimilar functioning conditions. Besides, extensive characterization tests were done for a comprehensive scope of operational situations. To understand the thermal behavior and analysis the performance and the reliance of the impacting parameters, including state of charge and current rates on the heat loss and total generated heat of the lithium-ion battery cell undergoing dissimilar functioning conditions, several discharges and charge current pulses with dissimilar current rates at different state of charge levels, which varies from 0% to 100% state of charge, were exerted to the lithium-ion battery cell by employing Maccor automated test system.

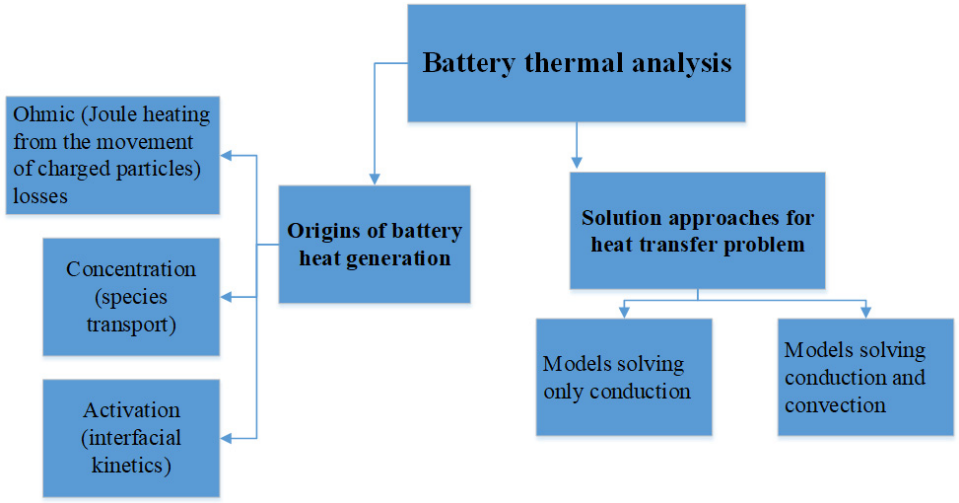

Figure 2. Origin and solution of heat production of lithium-ion batteries [40].

Table 2 demonstrates a complete description of the test matrix for Case A. Thermal characterizations of the lithium titanate oxide-based lithium-ion battery for case A are shown in Figure 3. In the case of A, two different current profiles were applied to the lithium titanate oxide-based lithium-ion battery. Eighteen different step time duration was considered for the state of charge. At 20 °C, charging from 29.3% to 33.1% state of charge, the heat generation was 0.604 Wh, 0.774 Wh, for 40 A, 50 A step charge rates. In the state of charge range of 29.3% to 69.6%, the average heat generation rate quantified for the lithium titanate oxide-based lithium-ion battery cell during 40 A and 50 A step charge cycles were 0.59 Wh and 0.74 Wh. Throughout the 50 A step discharge, the heat generation was higher than that of the 40 A step charge cycle throughout all the discharge processes. The maximum heat generation for 40 A and 50 A step charge cycles was from 0% state of charge to 29.3% state of charge. The minimum heat generation for 40 A step charge cycles was from 33.1% to 34.7% state of charge, while for 50 A, it was from 38.3% to 39.5% state of charge. The total generated heat variations displayed approximately a general rising pattern towards a significant state of charge for three dissimilar cases. For step 40 A charge, an increase of state of charge from 65 to 69.6 the transferred heat is 0.59 Wh while for step 50 A, this amount is 0.8 Wh.

Table 3 demonstrates a complete description of the test matrix for Case B. Thermal characterizations of a lithium titanate oxide-based lithium-ion battery for case B is demonstrated in Figure 4. In the case of B, three different current profiles were applied to the lithium titanate oxide-based lithium-ion battery. Seventeen different step time duration was considered for the state of charge. At 20 °C, discharging from 90.5% to 88.64% state of charge, the heat generation was 0.194 Wh, 0.676 Wh, and 1.038 Wh for 13 A, 40 A, and 100 A step discharge rates, respectively. In the state of charge range of 90.5% to 75.75%, the average heat generation rate quantified for the lithium titanate oxide-based lithium-ion battery cell during 100 A step discharge cycles was more significant by 0.33 Wh and 0.82 Wh than that observed for the 40 A and 13 A step discharge proportionately. Throughout the 100 A step discharge, the heat generation was remarkably higher than that of the 40 A and 13 A step discharge throughout the discharge process. The maximum heat generation for 13 A step discharge cycles was from 88.64% state of charge to 87% state of charge, and for 40 A and 100 A step discharge cycles were from 76.36% state of charge to 75.75% state of charge and 77.29% to 76.82% state of charge correspondingly. The minimum heat generation for 13 A step discharge cycles was from 78.5% to 78.07% state of charge while for 40 A, it was from 80.07% to 79.46% state of charge and for 100 A step discharge cycles were from 76.36% state of charge to 75.75% state of charge. This dissimilarity might correspond to phase alterations, charge transfer overpotentials, alterations in the system's heat capacity, and

other parameters. a decrease of SOC from 76.36 to 75.75 the transferred heat is 0.132 Wh, 0.77 Wh, and 0.62 Wh for 13 A, 40 A and 100 A step discharge accordingly.

Table 2. Test matrix for Case A.

Current	Cut-Off Voltage	State of Charge	Heat Generation	Current	Cut-Off Voltage	State of Charge	Heat Generation
3.25 A-CCC	1.500	0	2.368	3.25 A-CCD	2.543	90.820	3.791
3.25 A-CCD	2.800	100		3.25 A-CCC	1.500	0	
3.25 A-CCC	1.500	0		3.25 A-CCD	2.800	100	
40 A-PC	2.093	29.300	0.790	3.25 A-CCC	1.500	0	
40 A-PC	2.131	33.100	0.604	50 A-PC	2.093	29.300	1.109
40 A-PC	2.147	34.700	0.533	50 A-PC	2.131	33.100	0.774
40 A-PC	2.160	36	0.563	50 A-PC	2.147	34.700	0.695
40 A-PC	2.172	37.200	0.571	50 A-PC	2.160	36	0.698
40 A-PC	2.183	38.300	0.545	50 A-PC	2.172	37.200	0.693
40 A-PC	2.195	39.500	0.556	50 A-PC	2.183	38.300	0.684
40 A-PC	2.206	40.600	0.580	50 A-PC	2.195	39.500	0.678
40 A-PC	2.219	41.900	0.606	50 A-PC	2.206	40.600	0.698
40 A-PC	2.234	43.400	0.577	50 A-PC	2.219	41.900	0.714
40 A-PC	2.252	45.200	0.582	50 A-PC	2.234	43.400	0.720
40 A-PC	2.274	47.400	0.583	50 A-PC	2.252	45.200	0.720
40 A-PC	2.301	50.100	0.642	50 A-PC	2.274	47.400	0.730
40 A-PC	2.332	53.200	0.570	50 A-PC	2.301	50.100	0.750
40 A-PC	2.368	56.800	0.610	50 A-PC	2.332	53.200	0.710
40 A-PC	2.407	60.700	0.610	50 A-PC	2.368	56.800	0.730
40 A-PC	2.450	65	0.640	50 A-PC	2.407	60.700	0.760
40 A-PC	2.496	69.600	0.590	50 A-PC	2.450	65	0.760
40 A-PC	2.543	74.300	-	50 A-PC	2.496	69.600	0.800

Table 4 demonstrates a complete description of the test matrix for Case C. Thermal characterizations of a lithium titanate oxide-based lithium-ion battery for case C are illustrated in Figure 5. In the case of C, three different current profiles were applied to the lithium titanate oxide-based lithium-ion battery. Nineteen different step time duration was considered for the state of charge. The collected energy in the lithium-ion battery cells increased while it was greater charged or discharged. The aforementioned causes the heat flux curves to begin to swerve from each other, and the deviation raises at the end of the charge and discharges experiments. At 30 °C, discharging from 100% to 90.43% state of charge, the heat generation was 0.396 Wh, 0.437 Wh, and 0.498 Wh for 40 A, 50 A, and 60 A step discharge rates, respectively. It can be observed from Figure 5 that until the state of charge of 90.43%, heat generation rate curves for the 40 A, 50 A, and 60 A approximately overlap each other. As the energy collected in these cells is more discharged, the three curves commence deviating apart. By raising the lithium titanate oxide-based lithium-ion battery discharging and charging current rates, the electrochemical reaction velocity increases, causing more significant heat exchange and molecular interaction. In the state of charge range of 90.43% to 78.68%, the average heat generation rate quantified for the lithium titanate oxide-based lithium-ion battery cell during 60 A step discharge cycles was more significant by 0.068 Wh and 0.136 Wh than that observed for the 50 A and 40 A step discharge proportionately. A decrease of state of charge from 76.29 to 75.68 the

transferred heat is 0.416 Wh, 0.507 Wh, and 0.59 Wh for 40 A, 50 A, and 60 A step discharge accordingly.

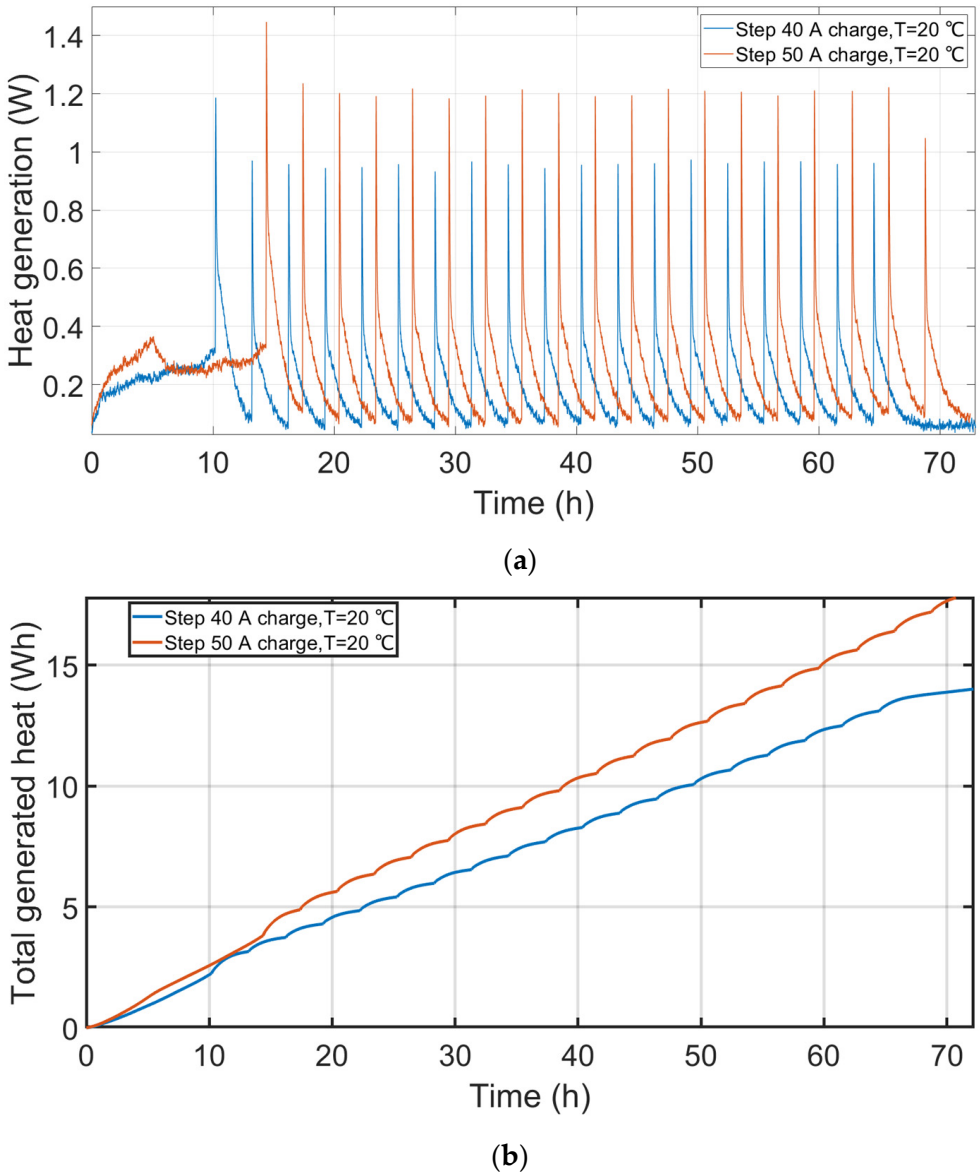

Figure 3. Thermal characterizations of a lithium titanate oxide-based lithium-ion battery, (**a**) heat generation evolution for case A, (**b**) Total generated heat for case A.

The maximum heat generation for 40 A, 50 A, and 60 A step discharge cycles was 76.29% state of charge to 75.68% state of charge. The minimum heat generation for 40 A step discharge cycles was from 86.93% to 85.43% state of charge, while for 50 A, it was from 84% to 82.79% state of charge and for 60 A step discharge cycles were from 100% state of charge to 90.43% state of charge. The heat generation during 20 °C was more significant than 30 °C. This could express the lithium titanate oxide-based lithium-ion battery cell's lesser internal resistance at a more significant temperature. Nevertheless, there was some exception for operational temperature 50 °C at individual current rates. The temperature gradient rises with current and declines with environment temperature. At lower working conditions, lesser heat is transferred in colder regions of the lithium titanate oxide-based battery cell than in hotter regions. At smaller temperatures, the exterior heat removal becomes greater attributable to the temperature variation between ambient and cell temperature. These alterations might be concerned with irreversible and reversible heat sources of the lithium titanate oxide-based lithium-ion battery cell with a dissimilar contribution.

Table 3. Test matrix for Case B.

Current	Cut-Off Voltage	State of Charge	Heat Generation	Current	Heat Generation	Current	Heat Generation
3.25 A-CCC	2.264	80.86	2.524	3.25 A-CCD	3.044	3.25 A-CCD	2.459
3.25 A-CCD	2.800	100		3.25 A-CCD		3.25 A-CCD	
3.25 A-CCC	1.500	0		3.25 A-CCC		3.25 A-CCC	
3.25 A-CCD	2.534	90.50		3.25 A-CCD		3.25 A-CCD	
13 A-PD	2.482	88.64	0.194	40 A-PD	0.676	100 A-PD	1.038
13 A-PD	2.436	87.00	0.231	40 A-PD	0.654	100 A-PD	1.071
13 A-PD	2.394	85.50	0.206	40 A-PD	0.645	100 A-PD	1.071
13 A-PD	2.355	84.11	0.166	40 A-PD	0.632	100 A-PD	1.020
13 A-PD	2.320	82.86	0.179	40 A-PD	0.633	100 A-PD	1.009
13 A-PD	2.290	81.79	0.194	40 A-PD	0.608	100 A-PD	1.003
13 A-PD	2.263	80.82	0.194	40 A-PD	0.618	100 A-PD	0.987
13 A-PD	2.242	80.07	0.141	40 A-PD	0.613	100 A-PD	0.982
13 A-PD	2.225	79.46	0.103	40 A-PD	0.587	100 A-PD	0.960
13 A-PD	2.210	78.93	0.152	40 A-PD	0.653	100 A-PD	1
13 A-PD	2.198	78.50	0.172	40 A-PD	0.697	100 A-PD	1.030
13 A-PD	2.186	78.07	0.098	40 A-PD	0.670	100 A-PD	0.990
13 A-PD	2.175	77.68	0.113	40 A-PD	0.660	100 A-PD	1
13 A-PD	2.164	77.29	0.201	40 A-PD	0.720	100 A-PD	1.120
13 A-PD	2.151	76.82	0.205	40 A-PD	0.720	100 A-PD	1.130
13 A-PD	2.138	76.36	0.181	40 A-PD	0.710	100 A-PD	0.850
13 A-PD	2.121	75.75	0.132	40 A-PD	0.770	100 A-PD	0.620

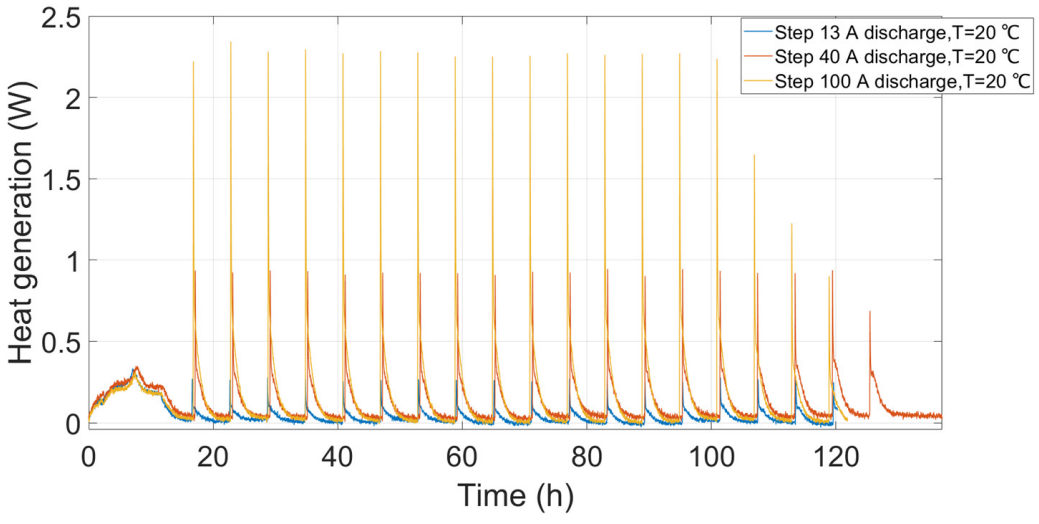

(**a**)

Figure 4. *Cont*.

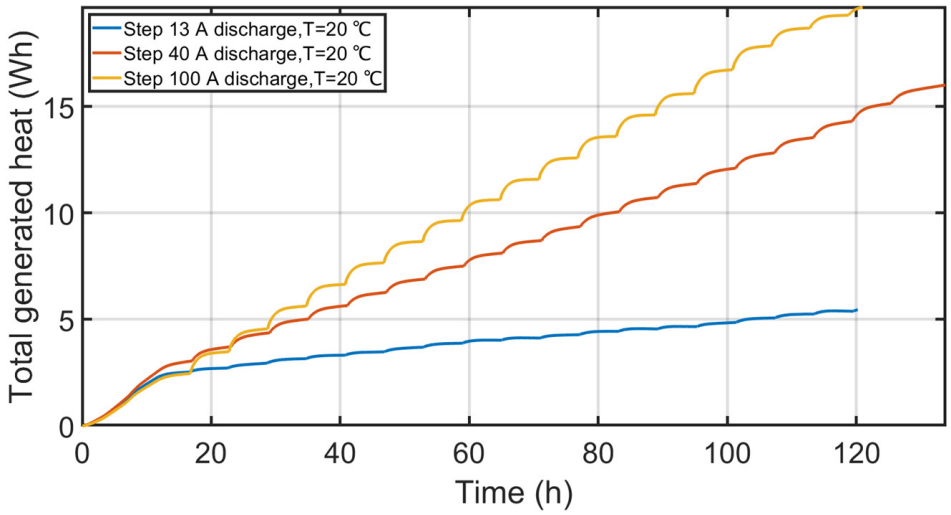

(**b**)

Figure 4. Thermal characterizations of a lithium titanate oxide-based lithium-ion battery, (**a**) heat generation evolution for case A, (**b**) total generated heat for case A.

Table 4. Test matrix for Case C.

Current	Cut-Off Voltage	State of Charge	Heat Generation	Current	Heat Generation	Current	Heat Generation
3.25 A-CCC	2.077	74.18	2.131	3.25 A-CCC	2.026	3.25 A-CCC	2.037
3.25 A-CCD	2.800	100		3.25 A-CCD		3.25 A-CCD	
3.25 A-CCC	1.500	0		3.25 A-CCC		3.25 A-CCC	
3.25 A-CCD	2.800	100		3.25 A-CCD		3.25 A-CCD	
40 A-PD	2.532	90.43	0.396	50 A-PD	0.437	60 A-PD	0.498
40 A-PD	2.480	88.57	0.375	50 A-PD	0.431	60 A-PD	0.499
40 A-PD	2.434	86.93	0.393	50 A-PD	0.428	60 A-PD	0.500
40 A-PD	2.392	85.43	0.360	50 A-PD	0.428	60 A-PD	0.507
40 A-PD	2.352	84.00	0.379	50 A-PD	0.457	60 A-PD	0.502
40 A-PD	2.318	82.79	0.377	50 A-PD	0.422	60 A-PD	0.506
40 A-PD	2.287	81.68	0.381	50 A-PD	0.441	60 A-PD	0.509
40 A-PD	2.262	80.79	0.376	50 A-PD	0.442	60 A-PD	0.518
40 A-PD	2.241	80.04	0.381	50 A-PD	0.452	60 A-PD	0.514
40 A-PD	2.223	79.39	0.379	50 A-PD	0.452	60 A-PD	0.509
40 A-PD	2.209	78.89	0.384	50 A-PD	0.445	60 A-PD	0.521
40 A-PD	2.196	78.43	0.383	50 A-PD	0.457	60 A-PD	0.527
40 A-PD	2.185	78.04	0.391	50 A-PD	0.462	60 A-PD	0.538
40 A-PD	2.174	77.64	0.387	50 A-PD	0.469	60 A-PD	0.512
40 A-PD	2.162	77.21	0.387	50 A-PD	0.460	60 A-PD	0.536
40 A-PD	2.150	76.79	0.394	50 A-PD	0.482	60 A-PD	0.557
40 A-PD	2.136	76.29	0.412	50 A-PD	0.492	60 A-PD	0.560
40 A-PD	2.119	75.68	0.416	50 A-PD	0.507	60 A-PD	0.590

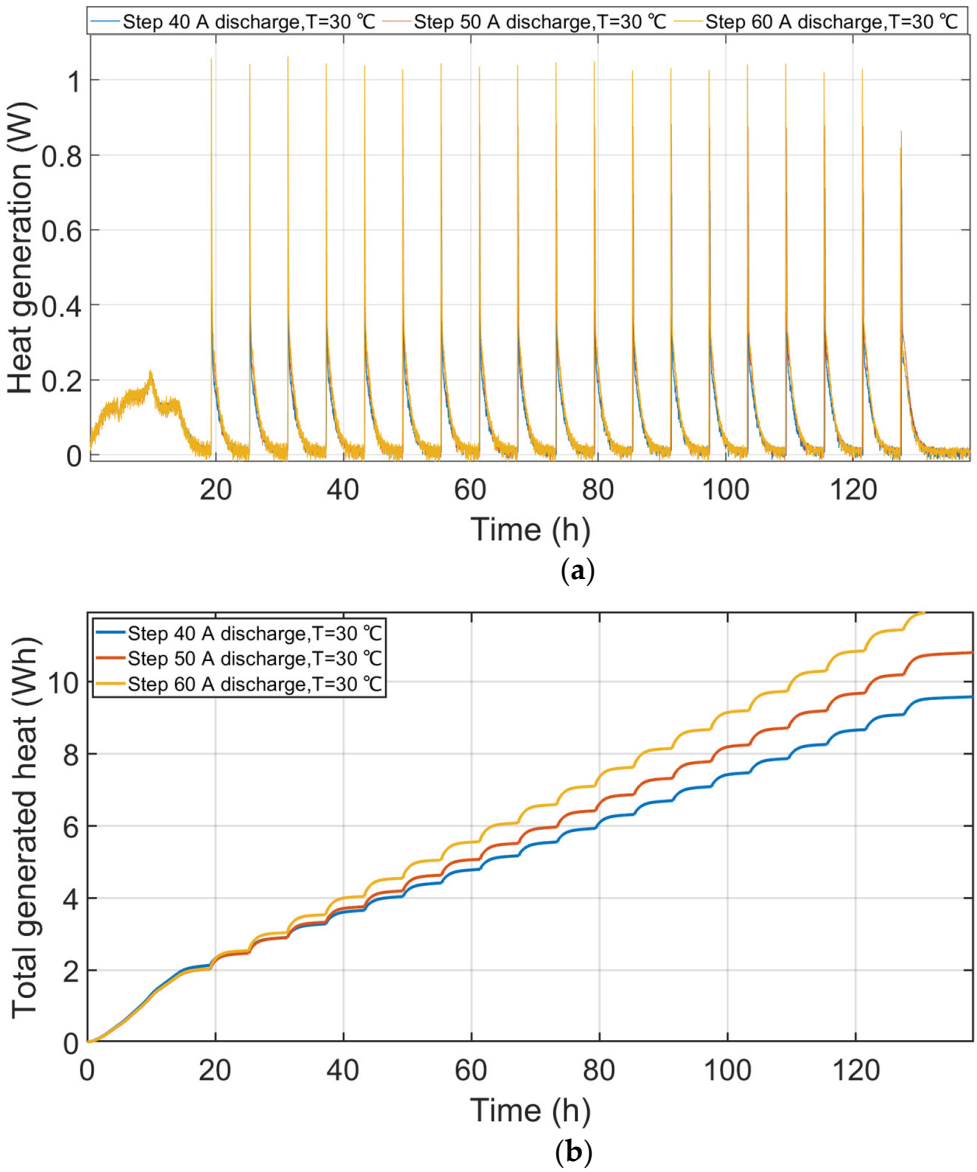

Figure 5. Thermal characterizations of a lithium titanate oxide-based lithium-ion battery, (**a**) heat generation evolution for case A, (**b**) total generated heat for case A.

A model was derived for the total generated heat of lithium-ion batteries, which comes from the isothermal battery calorimeter experiments. The thermal model equation was determined by MATLAB curve fitting tool by using experimental data. The R-square quantity for the total generated heat model is less than 0.9989. The total generated heat model parameters for different cases are exhibited in Table 5. The thermal model equation is presented in the following mathematical statement:

$$TGH(t) = A_1 \times \sin(B_1 \times t + C_1) + A_2 \times \sin(B_2 \times t + C_2) + A_3 \times \sin(B_3 \times t + C_3) + A_4 \times \sin(B_4 \times t + C_4) + A_5 \times \sin(B_5 \times t + C_5) + A_6 \times \sin(B_6 \times t + C_6) + A_7 \times \sin(B_7 \times t + C_7) + A_8 \times \sin(B_8 \times t + C_8) \quad (1)$$

where $TGH(t)$: Total generated heat (Wh) and t: time (h).

Figure 6 illustrates a comparison between different cases during random and periodic charge-discharge pulses. In case A for step 40 A charge, an increase of state of charge from 33.1 to 34.7 the transferred heat is 0.604 Wh is while for step 50 A, this amount is 0.774 Wh. In the case of B, a decrease of state of charge from 80.07 to 79.46 the transferred heat is 0.103 Wh, 0.587 Wh, and 0.96 Wh for 13 A, 40 A, and 100 A step discharge accordingly. In

case C, a decrease of state of charge from 79.39 to 78.89, the transferred heat is 0.384 Wh, 0.445 Wh, and 0.521 Wh for 40 A, 50 A, and 60 A step discharge accordingly.

Table 5. Parameters of the total generated heat model.

	Step 40 A Charge, 20 °C	**Step 50 A Charge, 20 °C**	**Step 13 A Discharge, 20 °C**	**Step 40 A Discharge, 20 °C**	**Step 100 A Discharge, 20 °C**	**Step 40 A Discharge, 30 °C**	**Step 50 A Discharge, 30 °C**	**Step 60 A Discharge, 30 °C**
A_1	5.33×10^7	6.20×10^7	2.35×10^7	5.86×10^7	6.82×10^7	3.57×10^7	3.89×10^7	4.23×10^7
B_1	1.02×10^{-5}	1.02×10^{-5}	7.28×10^{-6}	6.09×10^{-6}	6.18×10^{-6}	6.09×10^{-6}	5.80×10^{-6}	6.31×10^{-6}
C_1	−0.4048	−0.4048	−0.4579	−0.5172	−0.3037	−0.5144	−0.4207	−0.5416
A_2	1.90×10^7	1.90×10^7	9.22×10^6	2.27×10^7	2.53×10^7	1.35×10^7	1.48×10^7	1.61×10^7
B_2	2.00×10^{-5}	2.00×10^{-5}	1.45×10^{-5}	1.23×10^{-5}	1.19×10^{-5}	1.22×10^{-5}	1.14×10^{-5}	1.26×10^{-5}
C_2	1.67	1.67	1.022	1.254	2.049	1.241	1.606	1.265
A_3	2.73×10^6	2.73×10^6	1.64×10^6	3.75×10^6	4.68×10^6	2.20×10^6	2.56×10^6	2.86×10^6
B_3	3.93×10^{-5}	3.93×10^{-5}	2.93×10^{-5}	2.40×10^{-5}	2.30×10^{-5}	2.44×10^{-5}	2.20×10^{-5}	2.52×10^{-5}
C_3	2.409	2.409	0.7139	1.528	3.368	1.325	2.533	1.411
A_4	1.02×10^6	1.02×10^6	4.77×10^5	1.30×10^6	1.85×10^6	6.86×10^5	8.67×10^5	1.04×10^6
B_4	5.65×10^{-5}	5.65×10^{-5}	4.32×10^{-5}	3.64×10^{-5}	3.41×10^{-5}	3.66×10^{-5}	2.89×10^{-5}	3.79×10^{-5}
C_4	3.22	3.22	0.5231	1.568	4.465	1.396	4.56	1.515
A_5	7.44×10^5	7.44×10^5	1.33×10^5	4.84×10^5	9.23×10^5	2.46×10^5	3.62×10^5	4.72×10^5
B_5	8.29×10^{-5}	8.29×10^{-5}	7.60×10^{-5}	4.81×10^{-5}	4.22×10^{-5}	4.88×10^{-5}	4.32×10^{-5}	5.05×10^{-5}
C_5	2.418	2.418	−1.847	1.748	6.012	1.605	4.945	1.651
A_6	6.54×10^5	6.54×10^5	1.21×10^5	2.72×10^5	6.44×10^5	1.93×10^5	2.02×10^5	3.04×10^5
B_6	9.86×10^{-5}	9.86×10^{-5}	0.000289	0.0002867	0.0002903	0.0002926	0.0002842	0.0002902
C_6	3.264	3.264	0.6368	0.9783	0.6488	−2.78	−0.3131	−1.972
A_7	5.34×10^5	5.34×10^5	1.37×10^5	2.58×10^5	5.37×10^5	1.17×10^5	2.04×10^5	2.58×10^5
B_7	0.0001255	0.0001255	6.10×10^{-5}	5.20×10^{-5}	5.78×10^{-5}	0.0002816	0.0002955	6.31×10^{-5}
C_7	2.599	2.599	−0.4557	3.89	5.666	0.7229	2.741	1.824
A_8	3.39×10^5	3.39×10^5	8.69×10^4	1.82×10^5	3.96×10^5	1.17×10^5	1.82×10^5	1.86×10^5
B_8	0.0001314	0.0001314	0.0001307	0.0002944	6.48×10^{-5}	6.10×10^{-5}	4.99×10^{-5}	7.57×10^{-5}
C_8	5.069	5.069	1.966	−1.009	7.232	1.969	6.338	1.992

Such behavior and corresponding explanations about lithium titanate oxide batteries have not been reported in the literature. Only a few investigations reported the effect of the state of charge on heat generation of lithium-ion batteries. In [41], it was demonstrated that lithium-ion batteries' heat generation rate enhances discharging and charging rates. Generally, lithium-ion batteries' ohmic heat generation increases at significant discharge rates [42], notwithstanding reversible heat generation increases at a state of charge lower than twenty percent [43]. The overpotential lithium-ion batteries rise with decreasing state of charge by seventy-two percent at a discharge rate of 0.33C [44]. An experimental study [45] of lithium-ion batteries demonstrated that the entropic coefficient changed non-monotonically accompanied by a state of charge and raised considerably approaching the end state of charge lower than twenty-five percent.

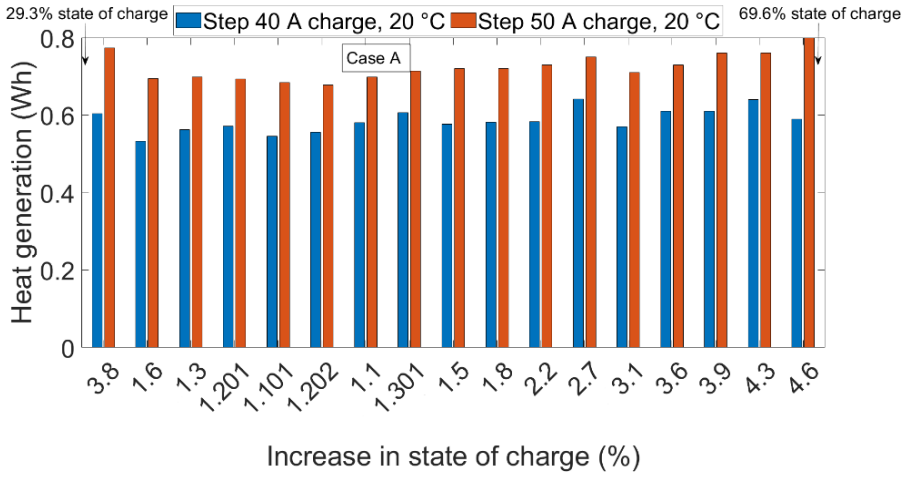

(**a**)

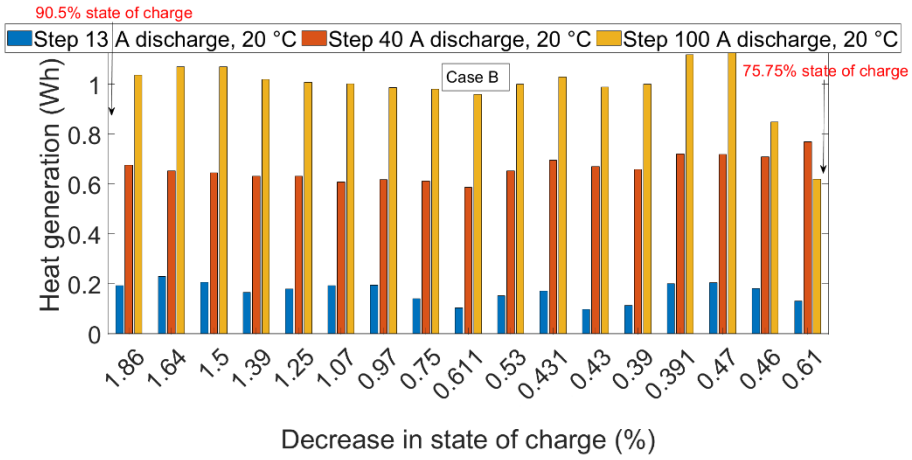

(**b**)

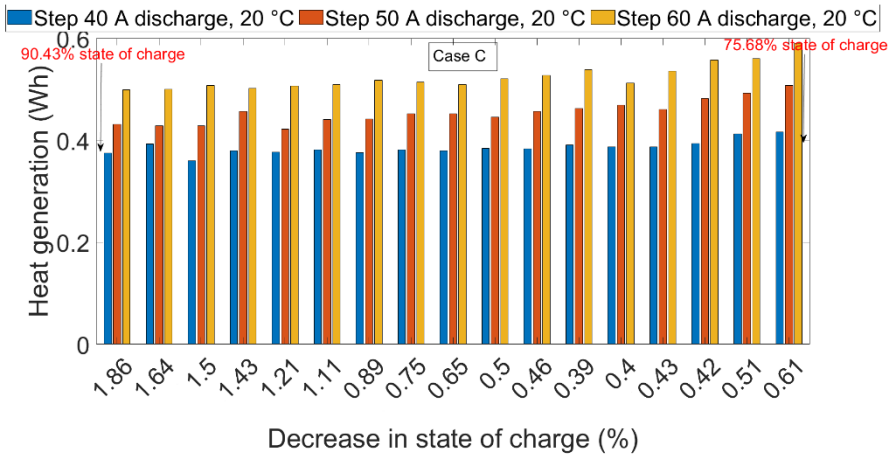

(**c**)

Figure 6. Comparison between different cases during random and periodic charge-discharge pulses: (**a**) case A, (**b**) case B, (**c**) case C.

4. Conclusions

The investigation, which was represented in this research, demonstrates a considerable scientific advancement and improvement in the comprehension of lithium-ion battery cells'

thermal behavior. The results can be used for different lithium-ion batteries' applications, including optimizing the thermal management of lithium-ion cells. Total heat generated exhibited a climbing pattern for all cases. Nevertheless, the rate of increase varied with state of charge level. The maximum heat generation during 40 A and 50 A pulse charges were 0.79 Wh and 1.109 Wh. Summarizing the results, it could be inferred that the experimental heat generations expressed nearly a climbing pattern towards a slight state of charge for all current rates. For case B, the difference between the total generated heat of 40 A and 50 A is approximately the same as 50 A and 60 A. This investigation has comprehensibly presented that the thermal energy, which was relocated during constant voltage and the current process, differs considerably from the accumulated thermal energy, which was transferred throughout stepped cycles. From the result of this study, it is feasible to infer that the amount of heat loss is related to the current rate and would contribute to lithium titanate oxide-based lithium-ion battery thermal modeling. It was demonstrated that even a small amount of decrease or increase in lithium-ion battery state of charge produces a considerable amount of heat. In case A for step 40 A charge an increase of state of charge from 43.4 to 45.2 the transferred heat is 0.582 Wh while for step 50 A charge this amount is 0.72 Wh. In the case of B, a decrease of state of charge from 90.5 to 88.64 the transferred heat is 0.194 Wh, 0.676 Wh, and 1.308 Wh for 13 A, 40 A, and 100 A step discharge accordingly. In case C, a decrease of state of charge from 90.43 to 88.57, the transferred heat is 0.375 Wh, 0.431 Wh, and 0.499 Wh for 40 A, 50 A, and 60 A step discharge accordingly. The significant impact of the initial and final state of charge, battery temperature, current rates, and state of charge on the lithium titanate oxide-based lithium-ion battery total generated heat was acknowledged using the experimental study. The influence of construction and chemistry of lithium titanate oxide-based lithium-ion battery on the total generated heat can be considered as future research. A comprehensive and detailed explanation of the proposed research works' simulation error, particularly the phenomena' reproducibility, will be accomplished in future investigations. This approach will make it simpler to advance the thermal model and apply it in lithium-ion batteries' system design tools, considering there is no necessity to integrate the electrochemical model with a thermal model to estimate heat generation.

Author Contributions: S.S.M. proposed the idea of the paper; S.S.M. wrote the paper; E.S. provided suggestions on the content and structure of the paper; S.K.K. and E.S. reviewed the draft manuscripts. All authors have read and agreed to the published version of the manuscript.

Funding: This research received no external funding.

Data Availability Statement: Not applicable.

Acknowledgments: Not applicable.

Conflicts of Interest: The authors declare no conflict of interest.

References

1. Ritchie, A.; Howard, W. Recent developments and likely advances in lithium-ion batteries. *J. Power Sources* **2006**, *162*, 809–812. [CrossRef]
2. Malik, M.; Dincer, I.; Rosen, M.A. Review on use of phase change materials in battery thermal management for electric and hybrid electric vehicles. *Int. J. Energy Res.* **2016**, *40*, 1011–1031. [CrossRef]
3. Hannan, M.A.; Hoque, M.M.; Mohamed, A.; Ayob, A. Review of energy storage systems for electric vehicle applications: Issues and challenges. *Renew. Sustain. Energy Rev.* **2017**, *69*, 771–789. [CrossRef]
4. Chauque, S.; Olivia, F.Y.; Visintin, A.; Barraco, D.; Leiva, O.R.; Camara, E.P.M. Lithium titanate as anode material for lithium ion batteries: Synthesis, posttreatment and its electrochemical response. *J. Electroanal. Chem.* **2017**, *799*, 142–155. [CrossRef]
5. Farmann, A.; Waag, W.; Sauer, D.U. Application-specific electrical characterization of high power batteries with lithium titanate anodes for electric vehicles. *Energy* **2016**, *112*, 294–306. [CrossRef]
6. Kim, J.; Oh, J.; Lee, H. Review on battery thermal management system for electric vehicles. *Appl. Therm. Eng.* **2019**, *149*, 192–212. [CrossRef]
7. Zhang, L.; Peng, H.; Ning, Z.; Mu, Z.; Sun, C. Comparative Research on RC Equivalent Circuit Models for Lithium-Ion Batteries of Electric Vehicles. *Appl. Sci.* **2017**, *7*, 1002. [CrossRef]

8. Zhang, S.S.; Xu, K.; Jow, T.R. The low temperature performance of li-ion batteries. *J. Power Sources* **2003**, *115*, 137–140. [CrossRef]
9. Choi, S.S.; Lim, H. Factors that affect cycle-life and possible degradation mechanisms of a Li-ion cell based on $LiCoO_2$. *J. Power Sources* **2002**, *111*, 130–136. [CrossRef]
10. Andre, D.; Meiler, M.; Steiner, K.; Wimmer, C.; Soczka-Guth, T.; Sauer, D.U. Characterization of high-power lithium ion batteries by electrochemical impedance spectroscopy. I. experimental investigation. *J. Power Sources* **2011**, *196*, 5334–5341. [CrossRef]
11. Pals, C.R.; Newman, J. Thermal modeling of lithium/polymer battery. I. discharge behavior of a single cell. *J. Electrochem. Soc.* **1995**, *142*, 3274–3281. [CrossRef]
12. Hall, F.; Touzri, J.; Wußler, S.; Buqa, H.; Bessler, W.G. Experimental investigation of the thermal and cycling behavior of a lithium titanate-based lithium-ion pouch cell. *J. Energy Storage* **2018**, *17*, 109–117. [CrossRef]
13. Pesaran, A.A.; Burch, S.D. Thermal Performance of EV and HEV Battery Modules and Packs Prepared under FWP HV71. *Fourteenth Int. Electr. Veh. Sump.* **1997**, *7*, 997.
14. Mariani, A.; D'Annibale, F.; Boccardi, G.; Celata, G.P.; Menale, C.; Bubbico, R.; Vellucci, F. Qualitative thermal characterization and cooling of lithium batteries for electric vehicles. *J. Phys. Conf. Ser.* **2014**, *501*, 1. [CrossRef]
15. Zhao, J.C.; Liu, S.H.; Zhang, J.F. Personalized distance learning system based on sequence analysis algorithm. *Int. J. Online Eng.* **2015**, *11*, 33–36. [CrossRef]
16. Wu, B.; Li, Z.; Zhang, J.; Huang, J.; Nie, Z.; Sun, Y.; An, F.; Wu, N. Thermal modelling of large-format laminated Li-ion battery and experimental validation using embedded thermocouples. In Proceedings of the 2013 World Electric Vehicle Symposium and Exhibition (EVS27), Barcelona, Spain, 17–20 November 2013; Volume 1, pp. 1–9.
17. Wang, Q.; Ping, P.; Zhao, X.; Chu, G.; Sun, J.; Chen, C. Thermal runaway caused Fire and explosion of lithium ion battery. *J. Power Sources* **2012**, *208*, 210–224. [CrossRef]
18. Lu, L.; Han, X.; Li, J.; Hua, J.; Ouyang, M. A review on the key issues for lithium-ion battery management in electric vehicles. *J. Power Sources* **2013**, *226*, 272–288. [CrossRef]
19. TLu, Y.; Chiang, C.C.; Wu, S.H.; Chen, K.C.; Lin, S.J.; Wen, C.Y.; Shu, C.M. Thermal hazard evaluations of 18650 lithium-ion batteries by an adiabatic calorimeter. *J. Therm. Anal. Calorim.* **2013**, *114*, 1083–1088.
20. Bhide, S.; Shim, T. Novel Predictive Electric Li-Ion Battery Model Incorporating Thermal and Rate Factor Effects. *IEEE Trans. Veh. Technol.* **2011**, *60*, 819–829. [CrossRef]
21. Zhao, X.W.; Zhang, G.Y.; Yang, L.; Qiang, J.X.; Chen, Z.Q. A new charging mode of batteries with $LiFePO_4$/C composites under low temperature. *J. Therm. Anal. Calorim.* **2011**, *104*, 561–567. [CrossRef]
22. Fleckenstein, M.; Bohlen, O.; Roscher, M.; Baker, B. Current density and state of charge inhomogeneities in li-ion battery cells with lifepo4 as cathode material due to temperature gradients. *J. Power Sources* **2011**, *196*, 4769–4778. [CrossRef]
23. Kameyama, H.; Hanamoto, T.; Ito, K.; Inui, Y.; Onda, K. Study on heat generation behavior of small lithium ion secondary battery. *IEEE Trans. Energy Convers.* **2001**, *112*, 1192–1199.
24. Onda, K.; Kameyama, H.; T, H.; Ito, K. Experimental study on the heat generation behavior of small lithium-ion secondary batteries. *J. Electrochem. Soc.* **2003**, *150*, A285. [CrossRef]
25. Karlsen, L.G.; Villadsen, J. Isothermal reaction calorimeters—I. A literature review. *Chem. Eng. Sci.* **1987**, *42*, 1153–1164. [CrossRef]
26. Cohen, R.; Melman, A.; Livne, N.; Peled, E. Heat Generation in Lithium-Thionyl Chloride and Lithium-SO_2 Cells. *J. Electrochem. Soc.* **1992**, *139*, 2386–2391. [CrossRef]
27. Kobayashi, Y.; Miyashiro, H.; Kumai, K.; Takei, K.; Iwahori, T.; Uchida, I. Precise Electrochemical Calorimetry of $LiCoO_2$/Graphite Lithium-Ion Cell. *J. Electrochem. Soc.* **2002**, *149*, A978. [CrossRef]
28. Sherfey, J.M. Calorimetric Determination of Half-Cell Entropy Changes. *J. Electrochem. Soc.* **1963**, *110*, 213. [CrossRef]
29. Chen, S.C.; Wan, C.C.; Wang, Y.Y. Thermal analysis of lithium-ion batteries. *J. Power Sources* **2005**, *140*, 111–124. [CrossRef]
30. Madani, S.S.; Schaltz, E.; Kær, K.S. An experimental analysis of entropic coefficient of a lithium titanate oxide battery. *Energies* **2019**, *12*, 2685. [CrossRef]
31. Madani, S.S.; Schaltz, E.; Kær, S.K. Investigation of the Effect of State-of-Charge and C-Rates on the Heat Loss and Efficiency of a Lithium-Ion Battery. *ECS Trans.* **2018**, *87*, 51–58. [CrossRef]
32. Madani, S.S.; Schaltz, E.; Kær, S.K. Thermal Modelling of a Lithium Titanate Oxide Batt. *ECS Trans.* **2018**, *87*, 315–326. [CrossRef]
33. Madani, S.S.; Schaltz, E.; Kær, S.K. Study of temperature impacts on a lithium-ion battery thermal behaviour by employing isothermal calorimeter. *ECS Trans.* **2018**, *87*, 295–305. [CrossRef]
34. Madani, S.S.; Schaltz, E.; Kær, S.K. Heat Loss Measurement of Lithium Titanate Oxide Batteries under Fast Charging Conditions by Employing Isothermal Calorimeter. *Batteries* **2018**, *4*, 59. [CrossRef]
35. Vertiz, G.; Oyarbide, M.; Macicior, H.; Miguel, O.; Cantero, I.; de Arroiabe, P.F.; Ulacia, I. Thermal characterization of large size lithium-ion pouch cell based on 1d electro-thermal model. *J. Power Sources* **2014**, *272*, 476–484. [CrossRef]
36. Nieto, N.; Díaz, L.; Gastelurrutia, J.; Alava, I.; Blanco, F.; Ramos, J.C.; Rivas, A. Thermal Modeling of Large Format Lithium-Ion Cells. *J. Electrochem. Soc.* **2013**, *160*, A212–A217. [CrossRef]
37. Eddahech, A.; Briat, O.; Vinassa, J.M. Thermal characterization of a high-power lithium-ion battery: Potentiometric and calorimetric measurement of entropy changes. *Energy* **2013**, *61*, 432–439. [CrossRef]
38. Abdul-Quadir, Y.; Laurila, T.; Karppinen, J.; Jalkanen, K.; Vuorilehto, K.; Skogström, L.; Paulasto-Kröckel, M. Heat generation in high power prismatic Li-ion battery cell with $LiMnNiCoO_2$ cathode material. *Int. J. Energy Res.* **2014**, *38*, 1424–1437. [CrossRef]

39. Xiao, M.; Choe, S.Y. Theoretical and experimental analysis of heat generations of a pouch type $LiMn_2O_4$/carbon high power Li-polymer battery. *J. Power Sources* **2013**, *241*, 46–55. [CrossRef]
40. Gümüşsu, E.; Ekici, Ö.; Köksal, M. 3-D CFD modeling and experimental testing of thermal behavior of a Li-Ion battery. *Appl. Therm. Eng.* **2017**, *120*, 484–495. [CrossRef]
41. Drake, S.J.; Martin, M.; Wetz, D.; Ostanek, J.K.; Miller, S.; Heinzel, J.; Jain, A. Heat generation rate measurement in a Li-ion cell at large C-rates through temperature and heat flux measurements. *J. Power Sources* **2015**, *285*, 266–273. [CrossRef]
42. Du, S.; Lai, Y.; Ai, L.; Ai, L.; Cheng, Y.; Tang, Y.; Jia, M. An investigation of irreversible heat generation in lithium ion batteries based on a thermo-electrochemical coupling method. *Appl. Therm. Eng.* **2017**, *121*, 501–510. [CrossRef]
43. Zhao, R.; Gu, J.; Liu, J. An investigation on the significance of reversible heat to the thermal behavior of lithium ion battery through simulations. *J. Power Sources* **2014**, *266*, 422–432. [CrossRef]
44. Arora, S.; Shen, W.; Kapoor, A. Critical analysis of open circuit voltage and its effect on estimation of irreversible heat for Li-ion pouch cells. *J. Power Sources* **2017**, *350*, 117–126. [CrossRef]
45. Manikandan, B.; Yap, C.; Balaya, P. Towards understanding heat generation characteristics of Li-Ion batteries by calorimetry, impedance, and potentiometry studies. *J. Electrochem Soc.* **2017**, *164*, A2794–A2800. [CrossRef]